Water-Gas Shift Modeling of Coal Gasification in an Entrained-Flow Gasifier

Xijia Lu * and Ting Wang
504-280-2398, 504-280-7183
xlv@uno.edu, twang@uno.edu
Energy Conversion& Conservation Center
University of New Orleans
New Orleans, LA 70148, USA

ABSTRACT

Most of the reaction rates for the water-gas shift (WGS) reaction were obtained from experiments under simplified laboratory conditions with specific catalysts. A few of the reaction rates without using catalysts were obtained under supercritical (water) conditions, with the pressure much higher than those in a typical gasifier. In either case, it is not clear how the published reaction rates can be trustfully used to predict the actual WGS reaction rate in a gasifier without the presence of a catalyst and under different temperature and pressure conditions than those in the laboratory. This study focuses first on reviewing the published WGS reaction rates with and without the presence of catalysts, followed by calibrating the WGS reaction rate to match the experimental data taken from the Japanese CRIEPI research gasifier. The 3-D Navier-Stokes equations and nine species transport equations are solved with seven global gasification reactions (three heterogeneous and four homogeneous,) and a two-step thermal cracking model for volatiles. The Chemical Percolation Devolatilization (CPD) model is used for the devolatilization process. Three different cases with three different finite rates for the WGS reaction (Jones's rate under catalytic conditions and Wade's and Sato's rates under non-catalytic conditions) are conducted. The result shows that the three originally published rates are all too fast and overpredict the experimental WGS reaction rate. Adding a backward WGS reaction rate doesn't slow down the reaction rate, resulting in the same gas composition and temperature at the gasifier exit as that calculated without adding the backward WGS reaction. The pre-exponential rate constant value (A) of each reaction rate is therefore adjusted to match the experimental data. The results show that all three WGS reaction rates can match the experimental data reasonably well. The exit temperature can be matched within 2% (20K). The mole fractions of CO and H_2O can be matched fairly well within 4 percentage points (or 10%); however, the simulated H_2 mole fractions are always 7-9 percentage points (or about 40%) higher than the experimental data. The suggested calibrated reaction rates are documented.

1. 0 INTRODUCTION

Gasification is an incomplete oxidation process of converting various carbon-based feedstocks into clean synthetic gas (syngas), which is primarily a mixture of hydrogen (H_2) and carbon monoxide (CO), with minor amounts of methane (CH_4) and inert nitrogen gas (N_2). Feedstock is partially combusted with oxygen and steam at high temperature and pressure with less than 30% of the required oxygen for complete combustion (i.e., the stoichiometric amount) being provided. The syngas produced can be used as a fuel (usually for boilers or gas turbines to generate electricity); it can also be made into a substitute natural gas (SNG), or hydrogen gas and/or other chemical products. Gasification technology is applicable to any type of carbon-based feedstock, such as coal, heavy refinery residues, petroleum coke, biomass, and municipal wastes. To help understand the gasification process in

gasifiers and subsequently use the learned knowledge to guide designs of more compact, more cost effective, and higher performance gasifiers, computational fluid dynamics (CFD) has been widely employed as a powerful tool to achieve these goals.

Chen et al. (2000) developed a three-dimensional simulation model for entrained-flow coal gasifiers, which applied an extended coal-gas mixture fraction model with the Multi Solids Progress Variables (MSPV) method. The model employed four mixture fractions separately track the variable coal off-gases from the coal devolatilization, char-O_2, char-CO_2, and char-H_2O reactions. Bockelie et al. (2002(a)) developed a comprehensive CFD modeling tool (GLACIER) to simulate entrained-flow gasifiers, including a single-stage, down-fired system and a two-stage system with multiple feed inlets. The U.S. Department of Energy/National Energy Technology Laboratory (NETL) developed a 3D CFD model of two commercial-sized coal gasifiers [Guenther and Zitney (2005)]. The commercial CFD software, FLUENT, was used to model the first gasifier, which was a two-stage, entrained-flow, slurry-fed coal gasifier. The Eulerian-Lagrangian method was used in conjunction with the discrete phase model to simulate the entrained-flow gasification process. The second gasifier was a scaled-up design of a transport gasifier. The NETL open source MFIX (Multiphase Flow Interphase eXchanges) Eulerian-Eulerian model was used for this dense multiphase transport gasifier. NETL has also developed an Advanced Process Engineering Co-Simulator (APECS) that combines CFD models and plant-wide simulation. APECS enables NETL to couple its CFD models with the steady-state process simulator, Aspen Plus.

From 2005 to 2011, Silaen and Wang have done a series of study of entrained-flow gasification process using the commercial CFD solver, FLUENT. Silaen and Wang (2005) investigated the effects of several parameters on gasification performance, including the coal input condition (slurry or dry powder), oxidant (oxygen-blown or air-blown), wall cooling, and various coal distributions between the two stages. The simulation results provide the temperature and species distributions inside the gasifier. In 2006, they investigated the effect of flow injection directions on the gasification performance using the same generic two-stage, entrained-flow gasifier. In 2010, they did research that investigated the effects of different parameters on gasification performance, including five turbulence models, four devolatilization models, and three solid coal sizes. With several improvements in the CFD modeling, including updating the finite rates for heterogeneous reactions, adding Chemical Percolation Devolatilization (CPD) devolatilization model, and adding two-stage volatiles cracking reactions, Silaen and Wang (2011) again conducted an investigation on the effects of different operation parameters in the gasification process, including the coal input condition (dry vs. slurry,) oxidant (oxygen-blown vs. air-blown,) and different coal distributions between the two stages.

In collaboration with the research team of Industrial Technology Research Institute (ITRI), Wang and Silaen effectively employed the CFD gasification model to investigate gasification process under the influences of different part loads, two different injectors, and three different slagging tap sizes (Wang, et al., 2006, 2007, and 2010). In 2011, Wang, et al. performed the simulation on the effects of potential fuel injection techniques on gasification performance in order to help design the top-loaded fuel injection arrangement for an entrained-flow gasifier using a coal-water slurry as the input feedstock. Two specific arrangements were investigated: (a) coaxial, dual-jet impingement with the coal slurry in the center jet and oxygen in the outer jet and (b) four-jet impingement with two single coal-slurry jets and two single oxygen jets.

One of the important reactions during the gasification process is the Water-Gas Shift (WGS) Reaction ($CO + H_2O \Leftrightarrow CO_2 + H_2$.) The WGS has been traditionally used for adjusting the H_2/CO ratio in a syngas to meet the specifications for various final products. The forward WGS reaction favors relatively low temperatures (under 600°C.) When the temperature is higher than 1200°C, the reverse reaction starts to dominate. This trend can be seen from the equilibrium constant shown in Table 1.

Table 1 Water-gas shift (WGS) reaction equilibrium balance constant

T(°C)	600	800	1000	1200	1400
$\log K_p$	1.396	0.553	0.076	-0.222	-0.424

The WGS reaction rate has been discovered to play an important role in affecting the accurate prediction of the syngas composition during simulations of the gasification process (Silaen and Wang, 2009). The earliest data recording the WGS reaction dates back to 1888 (Rhodes et al., 1995), and its prominence came with the Haber ammonia synthesis process and catalyst development by Bosch and Wilde in 1912 (Twigg, 1989). Most of the reaction rates for the WGS reaction were obtained from experiments with specific catalysts under laboratory conditions of relatively narrow ranges of pressure and temperature. A few of the reaction rates without using catalysts were obtained under various supercritical (water) conditions because a large excess of water solvent could possibly drive the reaction to produce hydrogen without a catalyst. However, the pressure under a supercritical condition is much higher than that in an operating gasifier. In either case, it is not clear how the published reaction rates can be trustfully used to predict the actual WGS reaction rate in a gasifier without the presence of catalysts and under different temperature and pressure conditions than those used in the laboratory. Due to the unavailability of appropriate WGS reaction rates for broad operating conditions in actual gasifiers, the **objective** of this study is to obtain an appropriate representative WGS global reaction rate under non-catalytic conditions by calibrating the WGS rate against the experimental data form an actual gasifier.

1.1 Review of WGS Reaction Rates

1.1.1 WGS Catalytic Reactions

Chen et al. (2008) investigated the characteristics of carbon monoxide conversion and hydrogen generation from the WGS reaction experimentally using a high-temperature catalyst and a low-temperature catalyst. The important parameters, including the catalyst type, residence time of the reactants in the catalyst bed, reaction temperature, and CO/steam ratio, were addressed as the influential factors that affected the performance of the WGS reaction. The experimental results showed that when the residence time was as long as 0.09s, the WGS developed well no matter which catalyst was used. It also revealed that the WGS reactions with the high-temperature catalyst and the low-temperature catalyst were governed by chemical kinetics and thermodynamic equilibrium.

It is difficult to narrow down the expression for the WGS reaction with a catalyst because the rate of the reaction is dependent on various parameters, including the composition of the catalyst, the active surface area and structure of the catalyst, the size of the catalyst, age of the catalyst, the operating

temperature and pressure, and the composition of the gases. Smith, et al. (2010) made a comprehensive review of research on the WGS reaction rate and the developments in modeling approaches for designing WGS reactors. They consolidated a listing of the various important kinetic expressions published for both the high temperature and the low temperature water-gas shift reactions along with the details of the make-up of the catalysts and the operating conditions at which the kinetics were obtained. Selected studies from Smith et al.'s review are shown in Table 2 -4.

Table 2 WGS Reaction Rate with Noble Metal Catalysts (Smith et al., 2010)

Catalyst	Opertating Conditions	Arrhenius Parameters		Reference
		A	E (kJ/mol)	
Ru	300°C-1000°C 0.008 to 0.05 contact time Coated on alumina support 5wt% loading	1.6×10^7 (1/s)	80	Wheeler et al. (2004)
Ru/Ceria		5.0×10^7 (1/s)	80	
Ni		8.0×10^7 (1/s)	85	
Ni/Ceria		1.7×10^8(1/s)	85	
Pd		4.0×10^6(1/s)	100	
Pd/Ceria		4.0×10^7(1/s)	100	
Pt		1.0×10^6(1/s)	80	
Pt/Ceria		2.5×10^7(1/s)	80	
Rh/SiO_2	350°C	3.23×10^6 (molecules/s/site)	22.8±2.5 (kcal/mole)	Grenoble et al. (1981)
Pt/Al_2O_3	270°C	1.9×10^6 (molecules/s/site)	19.6±2.5 (kcal/mole)	
Pt/SiO_2	340°C	1.9×10^6 (molecules/s/site)	19.1±0.8 (kcal/mole)	
Pt/C	340°C	3.84×10^6 (molecules/s/site)	25.5±1.4 (kcal/mole)	
$CuO.1CeO.8O_{2-y}$ (Cu ceria)	200°C - 350°C	1.8×10^3 (1/s)	61	Henrik et al. (2006)
$CuO.1CeO.8O_{2-y}$ (Cu ceria)	300°C - 350°C	4.0×10^3 (1/s)	78	

Table 3 WGS Reaction Rate with High-Temperature Catalysts (310°C-450°C) (Smith et al., 2010)

Catalyst	Operating Conditions	Arrhenius Parameters		Reference
		A	E (kJ/mol)	
Power plant data	1/4" × 3/8",2.20g/cm^3	9.4×10^7 (1/s)	21.4(kCal/gmol)	Rase (1977)
Fe_3O_4/Cr_2O_3	3-5bar, 573°C-633°C	ln A = 26.1	95	Keiski et al.(1996)
Fe_3O_4/Cr_2O_3 8wt% Cr_2O_3	1atm, 350°C-440°C	ln A = 11.5	112	Rhodes et al. (2003)
Fe_3O_4/Cr_2O_3	1bar, 380°C-450°C	ln A = 10.1±0.2	118±1	
Fe_3O_4/Cr_2O_3	6bar, 380°C-450°C	ln A = 12.0±0.2	124±1	
Fe_3O_4/Cr_2O_3	27bar, 350°C-450°C	ln A = 7.4±0.1	111±1	
80-95% Fe_3O_4, 5-10% Cr_2O_3, 1-5%CuO	1atm, 450°C	$10^{0.659}$(mol/gcat-s)	88	San et al. (2009)

Table 4 WGS Reaction Rate with Low-Temperature Catalysts (200°C-250°C) (Smith et al., 2010)

Catalyst	Opertating Conditions	Arrhenius Parameters		Reference
		A	E (kJ/mol)	
ICI 52-1 (Copper based catalyst) density=5.83g/cm^3	1atm, 200°C	K = 5.37 × 10^{-7} (mol/m^{2}s)/atm^{1+m}		Salmi et al. (1989)
Cu-ZnO-Al_2O_3 (EX-2248)Sud Chemie	200-250μm, 120-250°C	lnA = 12.6	47.4	Choi et al. (2003)
42% CuO-ZnO-Al_2O_3	123°C-175°C CO/H_2O=1/3	4.9 × 10^6 (S^{-1})	71	Henrik et al. (2006)
CuO-ZnO-Al_2O_3	1atm, 200°C	-	79	Koryabkina et al. (2003)

1.1.2 WGS non-catalytic reactions

The above studies reviewed by Smith, et al. (2010) are all involved with catalysts, whereas those studies without using catalysts were all conducted under supercritical (water) conditions. Watanabe et al. (2001) did the research on the partial oxidation of *n*-hexadecane at 673K in supercritical water and found that when a carbon to oxygen ratio of 3:1 was used, the CO concentration in the products could reach almost 40%. So, it is possible to use partial oxidation of hydrocarbons to produce CO via the WGS reaction. In other words, it is possible to develop a non-catalytic way of reforming hydrocarbons without using high temperatures (1073-1273K).

Hirth and Franck (1993) reported the equilibrium constant K_a of WGS reaction at 773-873K and 40MPa. It is also mentioned that K_a is largely different from that in the ideal gas state and the equilibrium shifted to the reactants' side with increasing pressure. Holgate et al. (1992) proposed a global rate expression of the WGS reaction by conducting experiments in non-catalytic, supercritical conditions at 712-866K at 24.6MPa, $R_{WGS} = 10^{2.6\pm1.2} \exp[(-67\pm11)/RT](CO)^{0.81\pm0.19}$.

Sato et al. (2004) studied the kinetics of the WGS reaction under non-catalytic, supercritical conditions (653-713K and 10-30MPa) with an initial CO/H_2O ratio of 0.03 in a flow-type reactor. By analyzing the rate constants obtained by their study and those reported previously, a global reaction model for the WGS reaction under supercritical conditions was proposed as $k = 10^{5.58\pm1.38} \exp(-1.16 \pm 0.19 \times 10^5/RT)$ /s at 10-59.6 MPa and 653-866K. Wade et al. (2008) conducted experiments on the WGS reaction non-catalytically in the temperature range of 770 to 1050 K with an operating pressure of 24 MPa. They obtained the rate constants of A = 2.512 x 10^5 and E = 1.325 x 10^5 J/k mol.

1.1.3 WGS reaction rates used in CFD modeling

Usually, there are two approaches to modeling the WGS reaction rate in CFD. The first approach is to use the detailed kinetics with both forward and backward elementary reactions. In this approach, the rates of the elementary reactions are usually too many to be calculated in the CFD model, so the reaction rates are calculated separately in another software package, like Chemkin, at each iteration as the local temperature and pressure change. The advantage of this approach is that it provides the most appropriate vehicle to model the correct kinetics for the reaction rates, while the disadvantages are that the elementary kinetics may not be adequately known and that it could be difficult to achieve convergence in CFD computation. The second approach is to use Global Reaction Rates that are obtained by experiments. Since the rates are global, the rates usually reflect the net rate between the difference of the forward and backward rates. The advantages are that the global rates simplify the

complex CFD modeling and conserve the computational power, while the disadvantages are that (a) the experimental data are usually obtained in relatively narrow temperature and pressure ranges, (b) the rates are usually obtained when the products are lean and the presence of other species commonly in a gasifier is nonexistent, and (c) there is still a lack of sufficient data covering the entire span of the temperature range for the gasification process.

Watanabe and Otaka (2006) performed a numerical simulation with the coal gasification model on the Japanese 2 tons/day, research scale coal gasifier supported by the Central Research Institute of Electric Power Industry (CRIEPI). The rate constants of the WGS reaction that they used is A = 2.75 x 10^{10} and E = 8.37 x 10^{7} J/kmol for the forward reaction rate and A = 2.65 x 10^{-2} and E = 3.96x 10^{3} J/kmol for the backward reaction rate. The influence of the air ratio on gasification performance, gas temperature distribution, and product gas composition were presented and discussed in their paper. The numerically simulated results were compared favorably with the experimental data, and most features of the gasification process were claimed to have been captured adequately. Ajilkumar et al. (2007) used the same WGS finite rate constant as employed by Watanabe and Otaka to simulate the same coal gasification process in the CRIEPI gasifier, but their computational domain was a small section of a simplified, axisymmetric cylinder (i.e. this was essentially a 2-D computation.) It was not clear how the inlet conditions and fuel injection were scaled down from 3D to 2D; however, they claimed that the predicted results showed good agreement with the experimental data of the CRIEPI gasifier. If Ajikumar et al.'s claim is correct, it implies that the gasfier's geometry and injection locations are not critical for designing a gasifier. Further studies are needed to verify this implication.

Silaen and Wang (2011) used Jones and Lindstedt's rate (1998, abbreviated as Jones's rate later) and compared their CFD-simulated syngas results with that from the actual production of a commercial, slurry-fed, entrained-flow coal gasifier fed from the bottom. Perhaps due to the fact that Jones's rate was obtained under catalytic conditions, they found that Jones's rate was too fast and they had to purposely reduce the reaction rate constant to A= 2.75 x 10^{2} to match the operating data. In this study, in addition to the modified Jones rate, the other two WGS reaction rates (Sato's and Wade's rates) obtained under non-catalytic conditions are to be employed for comparison as shown in Table 5.

Table 5 WGS Reaction Rates used in this study

Sources of the WGS rate	Catalyst	$k = AT^n \exp(-E/RT)$ with n=0
Jones and Lindstedt, 1998	Yes	$A = 2.75x10^{10}$, $E = 8.38x10^{7}$ J/kmol
Wade et al., 2008	No	$A = 2.512 \times 10^{5}$, $E = 1.325 \times 10^{5}$ J/kmol
Sato, et al. 2004	No	$A = 10^{5.58 \pm 1.38}$, $E = 1.16x\ 10^{5}$ J/kmol

1.1.4 Experimental data

In order to get an appropriate WGS reaction rate, detailed and accurate experimental data sets are needed to calibrate the CFD model. However, most of the experimental data available in the public domain was obtained after the syngas cooling or after the gas clean-up process. For limited data taken in the gasifier before the syngas cooling section, typically no information on the water vapor concentration is available. Lack of adequate "raw data" has made calibration of the gasification model and the WGS reaction rate uncertain and difficult. For example, the data of syngas composition published from the Wabash River Coal Gasification Repowering Project (2000, 2002) didn't show the

mole fraction of water vapor at the exit of the gasifier, although the water vapor information was shown for syngas composition after desulfurization. The experimental data provided by the Tampa Electric Polk Power Station IGCC Project (2002) was the cleaned syngas composition, which was taken after the syngas cooler and gas cleanup processes. Hughes et al. (2010) provided the syngas data from a two-tonne per day (slurry feed rate) pilot-scale gasifier, and, similarly, no water vapor mole fraction was given. Wained and Whitty (2010) performed tests in a 1 ton/day pressurized, slurry-fed, oxygen-blown, entrained-flow coal gasifier. The experimental data also lacked information for the water vapor content at the exit. So far, to the authors' knowledge, the only published experimental syngas data obtained before syngas cooling with water vapor content information is from the CRIEPI research scale coal gasifier presented in the paper by Watanabe and Otaka (2006). Therefore, the CRIEPI data is used for calibrating the WGS reaction rate in this paper.

1.2 Global Gasification Chemical Reactions

This study deals with the global chemical reactions of coal gasification (Smoot and Smith, 1985) that can be generalized in reactions (R1.1) through (R1.10) in Table 6.

Table 6 Summary of reaction rate constants used in this study

Reactions		Reaction Type	Reaction heat, $\Delta H°_R$ (MJ/kmol)	$k = AT^n\exp(-E/RT)$ (n=0)		Reference
				A	E(J/kmol)	
Heterogeneous Reactions						
R 1	$C(s) + ½\ O_2 \rightarrow CO$	Partial combustion	-110.5	0.052	6.1×10^7	Chen et al.(2000)
R 2	$C(s) + CO_2 \rightarrow 2CO$	Gasification, Boudouard reaction	+172.0	0.0732	1.125×10^8	
R 3	$C(s) + H_2O \rightarrow CO + H_2$	Gasification	+131.4	0.0782	1.15×10^8	
Homogeneous Reactions						
R 4	$CO + ½\ O_2 \rightarrow CO_2$	Combustion	-283.1	2.2×10^{12}	1.67×10^8	Westbrook and Dryer (1981)
R 5	**$CO+H_2O(g)\leftrightarrow CO_2+H_2$**	**Water Gas shift**	**-41.0**	**2.75×10^{10}**	**8.38×10^7**	**Jones and Lindstedt(1998)**
R 6	$CO + 3H_2 \leftrightarrow CH_4 + H_2O$	Methanation	-205.7	$k_f = 4.4\times10^{11}$	1.68×10^8	
				$k_b = 5.12\times10^{-14}$	2.73×10^4	Benyon P.(2002)
R 7	$CH_{2.2538}O_{0.3015} \rightarrow 0.3015CO + 0.3025H_2 + 0.3168CH_4 + 0.1908\ C_2H_2$	Two-step Volatiles Cracking	+12.088	Eddy dissipation		N/A
R 8	$CH_4 + ½O_2 \rightarrow CO+2H_2$	Volatiles gasification via CH_4	-35.71			
R 9	$C_2H_2 + O_2 \rightarrow 2CO + H_2$	Volatiles gasification via C_2H_2	-447.83			
R10	$H_2 + ½\ O_2 \rightarrow H_2O$	Oxidation	-242	6.8×10^{15}	1.68×10^8	Jones and Lindstedt (1998)
1) All $\Delta H°_R$ at 298K and 1 atm. 2) "+" Endothermic (absorbing heat), "-" Exothermic (releasing heat)						

In this study, the methanation reactions are not considered since the production of methane is negligible under the studied operating conditions. The volatiles are modeled to go through a two-step thermal cracking process (R1.7) and gasification processes (R1.8 and R1.9) with CH_4 and C_2H_2 as the intermediate products. The coal used in this study is Japanese Black Coal, whose compositions are given in Table 7. The compositions of volatiles are derived from the coal's heating value, proximate analysis, and ultimate analysis. The oxidant is considered to be a continuous flow and the coal particles are considered to be discrete. The discrete phase only includes the fixed carbon and liquid water droplets from the moisture content of coal (5.3% wt). Other components of the coal, such as N, H, S, O, and ash, are injected as gas, together with the oxidant in the continuous flow. N is treated as N_2, H as H_2, and O as O_2. S and ash are not modeled and their masses are lumped into N_2.

Table 7 Compositions of Japanese Black Coal

Proximate Analysis (MF), wt%		**Ultimate Analysis (MF), wt%**	
Volatile	46.8	C	68.2
Fixed Carbon	35.8	H	5.71
Moisture	5.3	O	12.26
Ash	12.1	N	0.99
	100	S	0.19
HHV (kJ/kg)	2.74×10^4	Ash	12.65
			100.00

2.0 COMPUTATIONAL MODEL

2.1 Governing Equations

The time-averaged, steady-state Navier-Stokes equations, as well as the mass and energy conservation equations, are solved. The governing equations for the conservations of mass, momentum, and energy are given as:

$$\frac{\partial}{\partial x_i}\left(\rho u_{i\,j}\right) = S_m \tag{1}$$

$$\frac{\partial}{\partial x_i}\left(\rho u_i u_j\right) = \rho \bar{g}_j - \frac{\partial P}{\partial x_j} + \frac{\partial}{\partial x_i}\left(\tau_{ij} - \rho\overline{u_i' u_j'}\right) + S_j \tag{2}$$

$$\frac{\partial}{\partial x_i}\left(\rho c_p u_i T\right) = \frac{\partial}{\partial x_i}\left(\lambda \frac{\partial T}{\partial x_i} - \rho c_p \overline{u_i' T'}\right) + \mu\Phi + S_h \tag{3}$$

where the symmetric stress tensor, τ_{ij}, is given by:

$$\tau_{ij} = \mu\left(\frac{\partial u_j}{\partial x_i} + \frac{\partial u_i}{\partial x_j} - \frac{2}{3}\delta_{ij}\frac{\partial u_k}{\partial x_k}\right). \tag{4}$$

The equation for species transport is given by:

$$\frac{\partial}{\partial x_i}\left(\rho u_i C_j\right) = \frac{\partial}{\partial x_i}\left(\rho D_i \frac{\partial C_j}{\partial x_i} - \rho\overline{u_i' C_j'}\right) + S_j\,. \tag{5}$$

2.2 Turbulence Models

The detailed analysis of the effect of various turbulence models on the gasification process has been documented in a previous paper by Silaen and Wang (2010). They compared the results of five turbulence models, including Standard k-ε, RNG (Re-Normalized Group) k-ε, Standard k-ω Model, Shear Stress Transport (SST) k-ω Model, and Reynolds Stress Model (RSM). They reported that the standard RSM model achieved the most consistent results and the k-ε turbulence model was found to yield reasonable results next to the RSM model, but the RSM model used almost seven times more computational time than the k-ε model. Following their conclusions without repeating the same process again, the standard k-ε turbulence model with enhanced wall function and variable material properties is used in this study to reduce the computational time.

2.3 Radiation Model

The P-1 radiation model is used to calculate the flux of the radiation at the inside walls of the gasifier. The P-1 radiation model is the simplest case of the more general P-N radiation model that is based on the expansion of the radiation intensity I. The P-1 model requires relatively little CPU demand and can easily be applied to various complicated geometries. It is suitable for applications where the optical thickness aL is large, where "a" is the absorption coefficient, and L is the length scale of the domain. In a gasifier, the optical thickness is thick due to the presence coal particles, soot, and ashes.

The heat sources or sinks due to radiation are calculated using the equation:

$$-\nabla q_r = aG - 4aG\sigma a^4 \qquad (6) \qquad \text{where} \quad q_r = -\frac{1}{3(a+\sigma_s)-C\sigma_s}\nabla G \qquad (7)$$

and q_r is the radiation heat flux, σ_s is the scattering coefficient, G is the incident radiation, C is the linear-anisotropic phase function coefficient, and σ is the Stefan-Boltzmann constant. The flux of the radiation, $q_{r,w}$, at the walls, caused by the incident radiation, G_w, is given as

$$q_{r,w} = -\frac{4\pi\pi_w \frac{\sigma T_w^4}{\pi} - (1-\rho_w)G_w}{2(1+\rho_w)} \qquad (8)$$

where ε_w is the emissivity and is defined as $\varepsilon_w = 1 - \rho_w$ and ρ_w is the wall reflectivity.

2.4 Discrete Phases (Coal Particles or Liquid Droplets)

Discrete phases include coal particles and liquid droplets. The Lagrangian method is adopted in this study to track each particle. Particles in the airflow can encounter inertia and hydrodynamic drag. Because of the forces experienced by a droplet in a flow field, the particles can be either accelerated or decelerated. The velocity change can be formulated by

$$m_p d\mathbf{v_p}/dt = \mathbf{F_d} + \mathbf{F_g} + \mathbf{F_o} \qquad (9)$$

where $\mathbf{F_d}$ is the drag of the fluid on the particle and $\mathbf{F_g}$ is the gravity. $\mathbf{F_o}$ represents the other body forces, which typically include the "virtual mass" force (such as centrifugal force, coriolis force, magnetic force, etc.), thermophoretic force, Brownian force, Saffman's lift force, etc. $V_\mathbf{p}$ is the particle velocity (vector). In this study, Saffman's lift force reaches about 30% of $\mathbf{F_g}$, so it is included in this study.

When the coal is injected through the injectors, the water content in the coal is treated as being in the condensed phase (i.e. liquid water), which can't be lumped into the continuous phase, so the liquid water is atomized into small droplets. Theoretically, evaporation occurs at two stages: (a) when the temperature is higher than the saturation temperature (based on the local water vapor concentration,) water evaporates from the droplet's surface, and the evaporation is controlled by the water vapor partial pressure until 100% relative humidity is achieved; and (b) when the boiling temperature (determined by the gas-water mixture pressure) is reached, water continues to evaporate even though the relative humidity reaches 100%. After the moisture is evaporated due to either high temperature or low moisture partial pressure, the vapor diffuses into the main flow and is transported away. The rate of vaporization is governed by the concentration difference between the surface and the gas stream, and the corresponding mass change rate of the droplet can be given by:

$$\frac{dm_d}{dt} = \pi d^2 k_c (C_s - C_\infty) \tag{10}$$

where k_c is the mass transfer coefficient and C_s is the concentration of the vapor at the particle's surface, which is evaluated by assuming that the flow over the surface is saturated. C_∞ is the vapor concentration of the bulk flow, obtained by solving the transport equations. The values of k_c can be calculated from empirical correlations by Ranz and Marshall (1952),

$$Sh_d = \frac{k_c d}{D} = 2.0 + 0.6 Re_d^{0.5} Sc^{0.33} . \tag{11}$$

where Sh is the Sherwood number, Sc is the Schmidt number (defined as ν/D), D is the diffusion coefficient of vapor in the bulk flow. Re_d is the Reynolds number, defined as $u\nu/d$, u is the slip velocity between the particle and the gas, and d is the particle diameter.

When the particle temperature reaches the boiling point, the following equation can be used to evaluate its evaporation rate:

$$\frac{dm_d}{dt} = \pi d^2 \left(\frac{\lambda}{d}\right)(2.0 + 0.46 Re_d^{0.5}) \ln\left(1 + c_p (T_\infty - T)/h_{fg}\right)/c_p \tag{12}$$

where $\lambda$is the heat conductivity of the gas/air, and h_{fg} is the droplet latent heat. c_p is the specific heat of the bulk flow.

The particle temperature can also be changed due to heat transfer between particles and the continuous phase. The particle's sensible heat changes depending on the convective heat transfer, latent heat (h_{fg}), species reaction heat (H_{reac}), and radiation, as shown in the following equation:

$$m_p c_p \frac{dT}{dt} = A_p h(T_\infty - T) + \frac{dm_p}{dt} h_{fg} + f_h \frac{dm_p}{dt} H_{reac} + A_p \varepsilon_p \sigma\left(\theta_R^{\,4} - T^4\right) \tag{13}$$

where the convective heat transfer coefficient (h) can be obtained with a similar empirical correlation to Eq. 14:

$$Nu_d = \frac{hd}{\lambda} = 2.0 + 0.6\, Re_d^{0.5}\, Pr^{0.33} \tag{14}$$

where Nu is the Nusselt number, and Pr is the Prandtl number. Eq. (13) is used for both water droplets and coal particles.

Stochastic Tracking of Particles -- The various turbulence models are based on the time-averaged equations. Using this flow velocity to trace the droplet will result in an averaged trajectory. In the real flow, the instantaneous velocity fluctuation would make the particle dance around this average track. However, the instantaneous velocity is not calculated in the current approach as the time averaged Navier-Stokes equations are solved. One way to simulate the effect of instantaneous turbulence on droplet dispersion is to use the stochastic tracking scheme. Basically, the particle trajectories are calculated by using the instantaneous flow velocity ($\bar{u}+u'$) rather than the average velocity ($\bar{u}$). The velocity fluctuation is then given as:

$$u' = \zeta\left(\overline{u'^2}\right)^{0.5} = \zeta(2k/3)^{0.5} \tag{15}$$

where ζ is a normally distributed random number. This velocity will apply during a characteristic lifetime of the eddy (t_e), given from the turbulence kinetic energy and dissipation rate. After this time period, the instantaneous velocity will be updated with a new ζ value until a full trajectory is obtained. When the stochastic tracking is applied, the basic interaction between the particles and the continuous phase remains the same, and is accounted for by the source terms in the conservation equations. The source terms are not directly, but rather indirectly affected by the stochastic method. For example, the drag force between particle and the airflow depends on the slip velocity calculated by the averaged Navier-Stokes equations if without the stochastic tracking. With stochastic tracking, a random velocity fluctuation is imposed at an instant of time, and the drag force and additional convective heat transfer will be calculated based on this instantaneous slip velocity. The source terms associated with this instantaneous drag force and convective heat transfer enter the momentum and energy equations without any additional formulation. For a steady-state computation, the "instant of time" means "each iteration step." Therefore, the averaged momentum equation will not be affected by the stochastic tracking scheme; rather the trajectory of the particle will reflect the effect of the imposed instantaneous perturbation.

2.5 Devolatilization Models

After all the moisture contained in the coal particle has evaporated, the particle undergoes devolatilization. Silaen and Wang (2010) compared the effect of four different devolatilization models on gasification process: namely the Kobayashi model, the single rate model, the constant rate model, and the CPD (Chemical Percolation Devolatilization) model [Fletcher and Kerstein (1992), Fletcher et. al (1990), and Grant et. al (1989)]. The analysis concluded that the rate calculated by the Kobayashi two-competing rates devolatilization model [H. Kobayashi et al.(1976)] is very slow, while that of the CPD model gives a more reasonable result. Therefore, the Chemical Percolation Devolatilization (CPD) model was chosen for this study. The CPD model considers the chemical transformation of the coal structure during devolatilization. It models the coal structure transformation as a transformation of a chemical bridge network, which results in the release of light gases, char, and tar. In this study, the volatiles contained in the coal are back calculated as $CH_{2.2538}O_{0.3015}$ from the coal heating value and coal composition in Table 7. The initial fraction of the bridges in the coal lattice is 1, and the initial fraction of char is 0. The lattice coordination number is 5. The cluster molecular weight is 400, and the side chain molecular weight is 50.

2.6 Reaction Models

2.6.1 Gas phase (homogeneous) reactions

For the gas phase reactions, both the eddy-dissipation and finite rates are used to calculate the reaction rate, and the smaller of the two rates is used in further calculation. The **Eddy-dissipation model** takes into account the turbulent mixing of the gases. It assumes that the chemical reaction is faster than the time scale of the turbulence eddies. Thus, the reaction rate is determined by the turbulence mixing of the species. The reaction is assumed to occur instantaneously when the reactants meet. The net rate of production or destruction of a species is given by the smaller of the two expressions below:

$$R = \nu' M A \rho \frac{\varepsilon}{k} \min\left(\frac{Y}{\nu' M}\right) \qquad (16) \qquad \text{and} \qquad R = \nu' M B \rho \frac{\varepsilon}{k} \min\left(\frac{\Sigma Y}{\Sigma \nu' M}\right) \qquad (17)$$

where ν′ is the stoichiometric coefficient of the reactant and ν′′ is the stoichiometric coefficient of the product. The smaller of the two expressions is used because it is the limiting value that determines the reaction rate.

The **finite rate** model does not take into account the turbulent mixing of the species. Instead, the reaction rate is expressed in an Arrhenius form. Reaction rates in Arrhenius form for all of the gas phase reactions are given in Table 6.

2.6.2 Heterogeneous reactions (coal particles)

The rate of depletion of the solid, due to surface reactions, is expressed as a function of the kinetic rate, the solid species mass fraction on the surface, and particle surface area. The reaction rates are all global net rates. Reaction rate constants used in this study are summarized in Table 6. Gasification and combustion of coal particles are dictated by the following global processes: (i) evaporation of moisture, (ii) devolatilization, (iii) gasification to CO and (iv) combustion of volatiles, CO, and char. The rate of depletion of solid due to a surface reaction is expressed as:

$$\overline{R} = A_p \eta Y R \qquad (18) \qquad \text{and} \qquad R = k\left(p_n - \frac{R}{D}\right)^N \qquad (19)$$

where

$\overline{R}$ = rate of particle surface species depletion (kg/s)
A_p = particle surface area (m^2)
Y = mass fraction of surface the solid species in the particle
η = effectiveness factor (dimensionless)
R = rate of particle surface species reaction per unit area (kg/m^2-s)
p_n = bulk partial pressure of the gas phase species (Pa)
D = diffusion rate coefficient for reaction
k = kinetic rate of reaction (units vary)
N = apparent order of reaction.

The kinetic rate of reaction is defined as:

$$k = A T^n e^{-(E/RT)} . \qquad (20)$$

The rate of particle surface species depletion for reaction order N = 1 is given by:

$$\overline{R} = A\eta Y p_n \frac{kD}{D+k} \cdot \quad (21)$$

For reaction order N = 0, $\overline{R} = A\eta Y k$. (22)

The effectiveness factor (η) is set unity (i.e., not being used) for an apparent reaction rate model.

2.7 Physical Characteristics of the Model and Assumptions

The geometry of the CRIEPI gasifier described by Watanabe and Otaka (2006) is shown in Fig 1. A simplified geometry shown in Figure 2 is employed in this present study without including the contraction section connecting the oxidation and reduction sections. The coal (fuel) injection design follows that of CRIEPI, consisting of a two-stage injection method with four tangential injections at the first stage and two opposite injections at the second stage. The residence time is around 3-4 seconds. The recycled char is injected from two opposite char injection locations at the first stage in the CFD model. The grid consists of 1,106,588 unstructured tetrahedral cells. In the simulations, the buoyancy force is considered, varying fluid properties are calculated for each species and the gas mixture, and the walls are assumed impermeable and adiabatic. The flow is steady and the no-slip condition (zero velocity) is imposed on the wall surfaces.

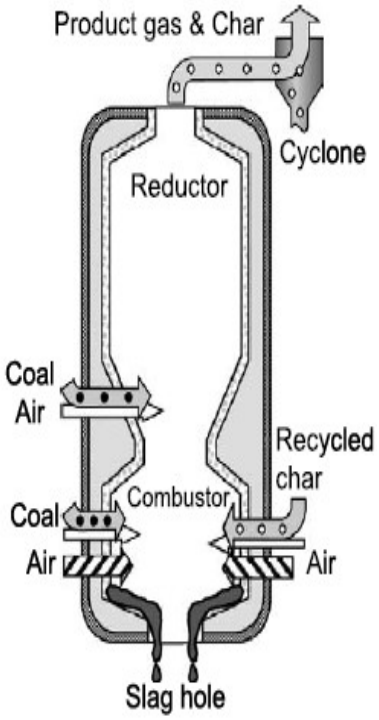

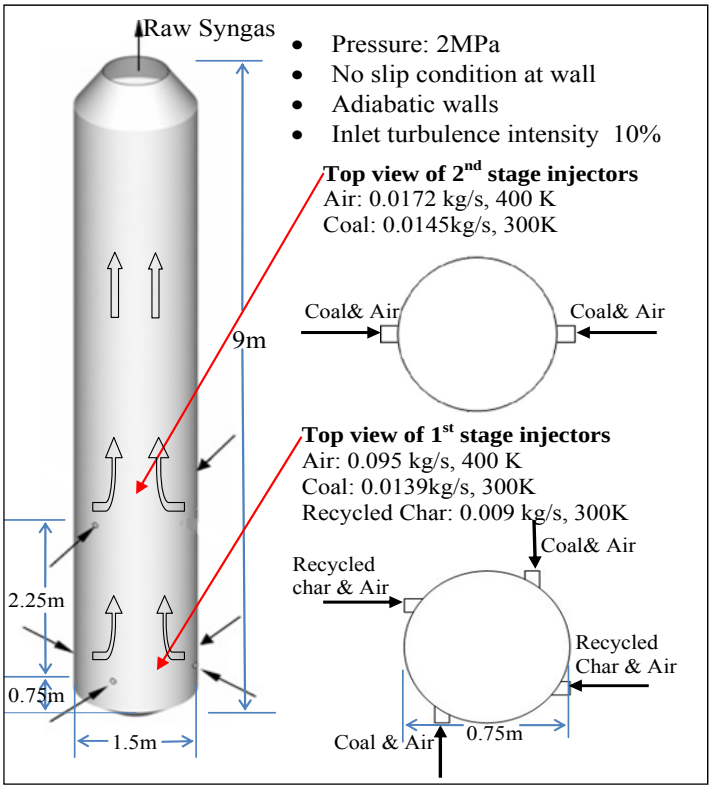

Fig. 1 CRIEPI research scale coal gasifier **Fig. 2 Boundary conditions of the simulated gasifier**

3.0 BOUNDARY AND INLET CONDITIONS

Japanese Black coal is used as the feedstock in this study; its composition is given in Table 7. The CRIEPI gasifier is an air-blown, dry-fed gasifier and is operated at 20 atm. The inlet, boundary, and

operating conditions for the baseline case are shown in Figure 2. At the first stage, coal is injected tangentially with a mass flow rate of 0.00695 kg/s at each injection location. The recycled char is injected oppositely with a mass flow rate of 0.0045 kg/s at each injector. The total mass flow rate of air is distributed into four injectors equally at 0.095 kg/s. At the second stage, coal is injected through a pair of opposite injectors with a mass flow rate 0.00725 kg/s at each injection location. The total mass flow rate of air is 0.0172 kg/s. All of the parameters stated above are the same as the experiment data.

The walls are all set to be adiabatic and with the no-slip condition (i.e. zero velocity). The boundary condition of the discrete phase at the walls is assigned as "reflect", which means the discrete phase elastically rebounds off once reaching the wall. The operating pressure inside the gasifier is set at 2MPa. The outlet is set at a constant pressure of 1 bar. The syngas is considered to be a continuous flow, and the coal and char from the injection locations are considered to be discrete particles. The particle size is uniformly given as spherical droplets with a uniform arithmetic diameter of 40 μm. Although the actual size distribution of the coal particles will be non-uniform, a simulation using uniform particle size provides a more convenient way to track the devolatilization process of coal particles than a non-uniform size distribution.

The computation is performed using the finite-volume-based commercial CFD software, FLUENT 12.0, from ANSYS, Inc. The simulation is steady-state and uses the pressure-based solver, which employs an implicit pressure-correction scheme and decouples the momentum and energy equations. SIMPLE algorithm is used to couple the pressure and velocity. The second-order upwind scheme is selected for spatial discretization of the convective terms. For the finite rate model, where the Eulerian-Lagrangian approach is used, the iterations are conducted by alternating between the continuous and the discrete phases. Initially, one iteration in the continuous phase is conducted followed by one iteration in the discrete phase to avoid having the flame die out. The iteration number in the continuous phase gradually increases as the flame becomes more stable. Once the flame is stably established, fifteen iterations are performed in the continuous phase followed by one iteration in the discrete phase. The drag, particle surface reaction, and mass transfer between the discrete and the continuous phases are calculated. Based on the discrete phase calculation results, the continuous phase is updated in the next iteration, and the process is repeated. Converged results are obtained when the residuals satisfy a mass residual of 10^{-3}, an energy residual of 10^{-5}, and momentum and turbulence kinetic energy residuals of 10^{-4}. These residuals are the summation of the imbalance in each cell, scaled by a representative for the flow rate. The computation is performed in a PC-cluster of 20 nodes.

4.0 RESULTS AND DISCUSSIONS

4.1 Results of Using Three Original Experimental WGS Reaction Rates.

The three original experimental WGS reaction rates shown in Table 5 are used first for comparison. In Watanabe and Otaka's paper (2006), the sum of the mole fractions of CO, CO_2, H_2O, and H_2 in the syngas composition is only 45%. The other 55% of the gases are not stated, although the major component is N_2. For the convenience of comparison between the experimental data and the CFD results, the mole fractions of CO, CO_2, H_2O, and H_2 are renormalized to 100% as shown in Table 8. The CFD results show that all three of the originally published rates are too fast, as can be seen by the much higher mole fraction of H_2 (product) and much lower mole fraction of remaining CO (reactant). Due to the exothermic character of the WGS reaction, the rapid WGS reaction rate results in the exit

temperatures of all three cases being 100 – 130 K higher than the experimental data. Based on this result, it is necessary to slow down the finite rate of the water shift reaction in order to match the experimental results better. The adopted approach is to keep the activation energy intact and subsequently reduce the pre-exponential constant value (A) until the CFD results match the experimental results. For Jones's rate, which was obtained under a catalytic condition, it could be explained that the WGS reaction rate is low because no catalyst is used in the gasifier. For Wade's rate and Sato's rate, there are two reasons that might partially contribute to the faster experimental reaction rates: (a) The experiments were conducted in an environment deprived of concentrations of products (H_2 and CO_2) and other gases, so the forward experimental reaction rates could be faster. (b) The experimental pressure and temperature conditions are different from those in the gasifier. In the gasifier, the temperature is higher than in the experimental conditions, thus the WGS reaction rate could be lower in the gasifier than in the experimental test condition. The temperature and species distributions in the gasifier are show in Fig. 3

Table 8 Comparison of exit temperature and syngas composition between the experimental data and the simulated cases using the 3 original WGS rates

Mole fraction	**Experimental Data**	**Jones's Rate $A=2.75\times10^{10}$ $E=8.38\times10^{7}$ J/kmol**	**Wade's Rate $A=2.512\times10^{5}$ $E=1.325\times10^{5}$ J/kmol**	**Sato's Rate $A=10^{5.58\pm1.38}$ $E=1.16\times10^{5}$ J/kmol**
T	1250K	1356K	1382K	1378K
H_2	0.20	0.48	0.48	0.48
CO	0.42	0.27	0.26	0.27
CO_2	0.20	0.25	0.26	0.25
H_2O	0.18	< 0.01	< 0.01	< 0.01

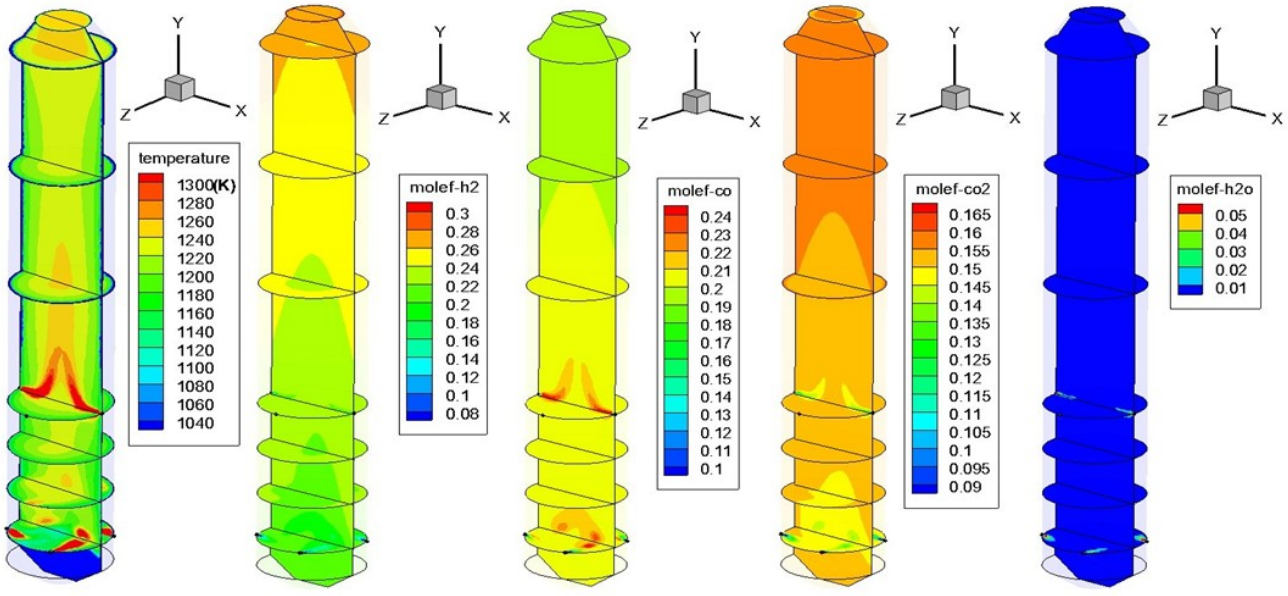

Fig. 3 Gas temperature and species mole fraction distributions for using the Jones's rate ($A=2.75\times10^{10}$ $E=8.38\times10^{7}$ J/kmol) (Note: the mole fractions in this figure are based on all gases and are not the same as those shown in Table 8.)

4.1.1 Backward WGS reaction rate

The backward WGS reaction rate is added to the Jones's rate with A = 2.65 x 10^{-2} and E = 3.96x 10^3 J/kmol (Gururajan et al., 1992). The result shows that adding this backward WGS reaction rate doesn't slow down the reaction rate during computation, resulting in the same gas composition and temperature at the gasifier exit as those data without adding the backward WGS reaction in Table 8. The backward WGS reaction rate is therefore not added to the rest of cases.

4.2 Calibration of the Catalytic WGS Rates (Jones's) Against the Experimental Data

The calibration against the experimental data is performed by consecutively changing the pre-exponential rate constant, A, from 2.75 x10^{10} in Jones's rate to 2.75 x 10^{-2}, while the activation energy is kept the same as the original value (E = 8.38x10^7 J/kmol.) The CFD results of seven cases are shown in Table 9 together with the experimental data. The result clearly shows the gradual change of syngas composition and temperature at the exit when the A value is reduced from 2.75 x 10^{10} to 2.75 x 10^{-2}. There is little change in syngas composition and temperature at the exit when the rate constant A is reduced from 2.512 x 10^{10} to 2.512 x 10^4 because the water vapor content is almost completely consumed in both cases. It demonstrates that the rate A = 2.512 x 10^4 is still too fast compared to the experimental data. There is a relatively large change of the gas composition when the rate constant A is reduced from 2.75 x 10^2 to 2.75. When the A-value is reduced below 2.75, the result appears stabilized and fluctuates slightly. The case with **A=2.75** seems to result in the best match with the experimental data.

Table 9 Comparison of the temperature and syngas composition at exit with the experimental data by consecutively reducing the pre-exponential value, A, of the Jones's rate

Exit	Exp. Data	2.75x10^{10}	2.75x10^4	2.75x10^2	2.75x10^1	**2.75**	2.75x10^{-1}	2.75x10^{-2}
T	1250K	1356K	1296K	1282K	1278K	**1267K**	1246K	1236K
H_2	0.20	0.48	0.44	0.41	0.31	**0.27**	0.29	0.27
CO	0.42	0.27	0.31	0.32	0.41	**0.45**	0.44	0.45
CO_2	0.20	0.25	0.25	0.23	0.14	**0.12**	0.12	0.12
H_2O	0.18	< 0.01	< 0.01	0.05	0.14	**0.16**	0.15	0.16

Figure 4 shows the gas temperature and species mole fraction distributions for the Case with A=2.75 and E=8.38x10^7 J/kmol. The gas temperature is higher in the region above the second stage injection location than it is in the region between the first and second stages. The maximum gas temperature in the first stage reaches 1650K near the fuel injection locations, and, in the second stage, it reaches 1570K. This phenomenon is different from the well-known E-gas gasifier in which no oxygen is provided at the second stage, so the temperature after the second-stage injection is much lower than in the first stage because the endothermic Char-CO_2 (R2) and Char-steam (R3) gasification processes are very active after the second stage injection. In this gasifier, it is very interesting to see that the highest production of CO_2 occurs near the first stage injection locations and the lowest production occurs near the second stage. The CO_2 mole fraction is low in most parts of the production until the syngas reaches the top quarter of the gasifier where the CO_2 mole fraction increases again. This history of the CO_2 mole fraction changes indicates that complete char combustion (R4) occurs near the first-stage injection, but CO_2 is effectively consumed via Char-CO_2 gasification in most parts

of the gasifier to produce H_2 and CO, as also is evidenced by increasing H_2 and CO mole fractions. The WGS seems to become more active in the upper quarter of the gasifier as the temperature increases due to the exothermic effect of the WGS process. In this upper quarter region, the active WGS reaction can be evidenced by the increased H_2 and CO_2 and decreased CO.

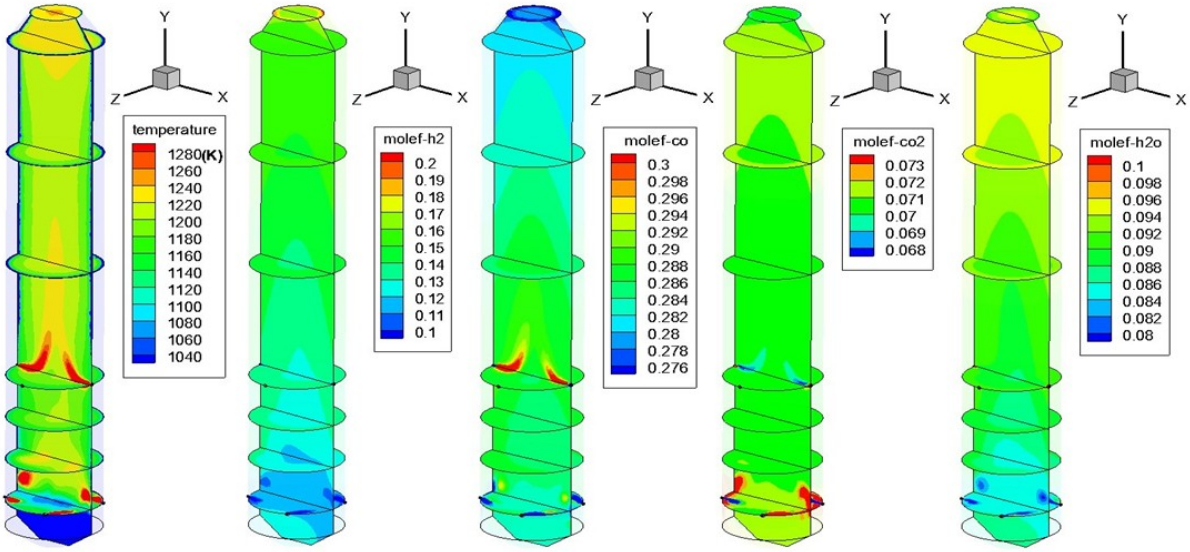

Fig. 4 Gas temperature and species mole fraction distributions for the Case with modified Jones's rate (A=2.75 and E=8.38x10^7 J/kmol). (Note: the mole fractions in this figure are based on all gases and are not the same as those shown in Table 9.)

4.3 Calibration of the Non-catalytic WGS Rates (Wade's and Sato's) Against the Experimental Data

The same calibration process is performed for Wade's and Sato's rates, which were obtained without using catalysts, but in the supercritical range. Without showing all the incremental cases, only three selected cases are shown in Table 10. The results of A = 2.512 x 10^{-3} for Wade's rate and A = 1 x 10^{-3} for Sato's rate show the best matches with the experimental data.

Table 10 Temperature and syngas composition at exit for six cases and experiment data based on Wade's rate and Sato's rate

MF		A-value of Wades' Rate (E=1.325x10^{5}J/kmol)			A-value of Sato's Rate (E=1.16x10^5 J/kmol)		
(%)	Exp. Data	2.512x10^5	2.512x10^{-1}	**2.512x10^{-3}**	$10^{5.58\pm1.38}$	1x10^{-1}	**1x10^{-3}**
T	1250K	1382K	1280K	**1273K**	1378K	1276K	**1238K**
H_2	0.20	0.48	0.43	**0.29**	0.48	0.40	**0.28**
CO	0.42	0.26	0.29	**0.43**	0.27	0.33	**0.46**
CO_2	0.20	0.26	0.24	**0.12**	0.25	0.21	**0.11**
H_2O	0.18	0	0.04	**0.16**	0	0.06	**0.15**

In Summary, all three WGS reaction rates can match the experimental data reasonably well by reducing the value of the pre-exponential rate constant, A. The exit temperature can be matched within 2% (20K) of the experimental value. The mole fractions of CO and H_2O can be matched fairly well within 4 percentage points (or 10%); however, the simulated H_2 mole fractions are always 7-9 percentage points (or about 40%) higher than the experimental data.

5.0 CONCLUSIONS

The WGS reaction rate has been discovered to notably affect the result of CFD modeling of coal gasification processes in a gasifier. Almost all of the published WGS rates were conducted with catalysts under limited temperature ranges and at a certain fixed pressure condition. Only a few WGS rates were obtained without involving catalysts, but they were performed under supercritical (water) conditions. Therefore, employing any of the published WGS reaction rates to simulate the coal gasification process in a gasifier, which usually doesn't use catalysts and doesn't operate at the same temperature or pressure conditions as in the laboratory conditions, is destined to result in misleading or uncertain results. To help calibrate the global WGS reaction rate, three published WGS reaction rates are used in this study. They are Jones's rate ($A = 2.75x10^{10}$, $E = 8.38x10^7$ J/kmol,) Wade's rate ($A = 2.512 \times 10^5$, $E = 1.325 \times 10^5$J/kmol,) and Sato's rate ($A = 10^{5.58, \pm 1.38}$ $E = 1.16x\ 10^5$ J/kmol.) The experimental data are from the air-blown, dry fed, 2-stage, research-scale gasifier operated by the Central Research Institute of Electric Power Industry (CRIEPI). The conclusions are:

(1) All of the originally published rates are too fast. Adding a backward WGS reaction rate doesn't slow down the reaction rate too much, resulting in the same gas composition and temperature at the gasifier exit as the case without adding the backward WGS reaction rate.

(2) Each of the three rates are slowed down by consecutively reducing the pre-exponential rate constant, A, while the activation energy is kept the same as the original value. The results show that all three WGS reaction rates can match the experimental data reasonably well by reducing the value of the pre-exponential rate constant, A. The exit temperature can be matched within 2% (20K). The mole fractions of CO and H_2O can be matched fairly well within 4 percentage points (or 10%); however, the simulated H_2 mole fractions are always 7-9 percentage points (or about 40%) higher than the experimental data.

(3) The calibrated global WGS reaction rates that best match the experimental data are:
- Modified Jones's rate: $A = 2.75$, $E = 8.38x10^7$ J/kmol
- Modified Wade's rate: $A = 2.512 \times 10^{-3}$, $E = 1.325 \times 10^5$J/kmol and
- Modified Sato's rate: $A = 1 \times 10^{-3}$, $E = 1.16x\ 10^5$ J/kmol

It needs to be emphasized that the calibrated reaction rates are obtained under air-blown and dry-fed operating conditions. These calibrated rates may not be applicable to slurry-fed or oxygen-blown gasifiers because the higher water vapor concentration in slurry-fed gasifiers and higher operating temperatures in oxygen-blown gasifiers may affect the global WGS rate. More studies are needed in the future, and more adequate experimental data is needed. The adequate data are those data taken immediately at the end of gasification section, but right before the syngas cooling section in the gasifier, and the water vapor concentration must be included. An alternative approach is to include the

kinetics of elementary reactions instead of taking a global data match on the condition that the adequate elementary reactions are known.

6.0 ACKNOWLEDGMENT

This study was partially supported by the Louisiana Governor's Energy Initiative via the Clean Power and Energy Research Consortium (CPERC) and was administered by the Louisiana Board of Regents and partially supported by the U.S. Department of Energy.

7.0 REFERENCES

Benyon P., 2002, "Computational Modelling of Entrained Flow Slagging Gasifiers," PhD thesis, School of Aerospace, Mechanical & Mechatronic Engineering, University of Sydney, Australia, 2002.

Bockelie, M.J., Denison, K.K., Chen, Z., Linjewile, T., Senior, C.L., and Sarofim, A.F., 2002, "CFD Modeling for Entrained Flow Gasifiers in Vision 21 Systems," Proceedings of the 19th Annual International Pittsburgh Coal Conference, Pittsburgh, PA. September 24-26, 2002

Chen, C., Horio, M., and Kojima, T., 2000, "Numerical Simulation of Entrained Flow Coal Gasifiers. Part I: Modeling of Coal Gasification in an Entrained Flow Gasifier", Chemical Engineering Science, Vol. 55, 3861-38740.

Chen, C., Horio, M., and Kojima, T., 2010, "Numerical Simulation of Entrained Flow Coal Gasifiers," Chemical Engineering Science, Vol. 55, pp. 3861-3883

Chen, W.H., Hsieh, T.C., and Jiang, T.L., 2008, "An Experimental Study on Carbon Monoxide Conversion and Hydrogen Generation from Water Gas Shift Reaction," Energy Conversion and Management, Vol. 49, pp. 2801-2808

Choi, Y., and Stenger, H.G., 2003, "Water Gas Shift Reaction Kinetics and Reactor Modeling for Fuel Cell Grade Hydrogen," Journal of Power Sources, Vol. 124, pp. 432–439

Fletcher, T.H., Kerstein, A.R., Pugmire, R.J., and Grant, D.M., 1990, "Chemical Percolation Model for Devolatilization: 2. Temperature and Heating Rate Effects on Product Yields," Energy and Fuels Vol. 4, pp.54-60

Fletcher, T.H., and Kerstein, A.R., 1992, "Chemical Percolation Model for Devolatilization: 3 Direct Use of ^{13}C NMR Date to Predict Effects of Coal Type," Energy and Fuels, Vol. 6, pp. 414-431

Grant, D.M., Pugmire, R.J., Fletcher, T.H., and Kerstein, A.R., 1989, "Chemical Percolation of Coal Devolatilization Using Percolation Lattice Statistics," Energy and Fuels, Vol. 3 pp. 175-186

Grenoble, D.C. and Estadt, M.M, 1981, "The Chemistry and Catalysis of the Water Gas Shift Reaction 1, the Kinetics over Supported Metal Catalysts," Journal of Catalysis, Vol. 67, pp. 90-102

Gururajan, V. S., Agarwal, P. K., and Agnew, J. B., 1992, " Mathematical modelling of fluidized bed coal gasifiers," Chemical engineering research & design, vol. 70, No. A3, p.p. 211-238, ISSN : 0263-8762

Hirth, T., and Franck, E.U., 1991, "Oxidation and Hydrothermolysis of Hydrocarbons in Supercritical Water at High Pressures," Ber. Bunsenges. Phys. Chem., Vol. 97, pp. 1091-1097

Hla, S.S., Park, D., Duffy, G.J., Edwards, J.H., Roberts, D.G., Ilyushechkin, A., Morpeth, L.D., and Nguyen, T., 2009, "Kinetics of High-temperature Water-Gas Shift Reaction over Two Iron-based Commercial Catalysts Using Simulated Coalderived Syngases," Chemical Engineering Journal, Vol. 146, pp. 148–154

Holgate, H.R., Webley, P.A., and Tester, J.W., 1992, "Carbon Monoxide Oxidation in Supercritical Water: the Effects of Heat Transfer and the Water-Gas-Shift Reaction on Observed Kinetics," Energy & Fuels, Vol.6, pp. 586-597

Hughes, R., Lu, D., Majeski, A., Corber, A., and Anthony, B., 2010, "Entrained Flow Slagging Slurry Gasification and the Development of Computational Fluid Dynamics Models at CanmetENERGY", 2010 International Pittsburgh Coal Conference, Istanbul, Turkey October 11 – 14, 2010.

Jones, W.P., and Lindstedt, R.P., 1998, "Global Reaction Schemes for Hydrocarbon Combustion," Combustion and Flame, Vol. 73, pp. 233

Keiski, R.L., Salmi, T., Niemisto, P., Ainassaari, J., and Pohjola, V.J., 1996, "Stationary and Transient Kinetics of the High Temperature Water Gas Shift Reaction," Applied Catalysis A: General, Vol. 137, pp. 349-370

Kobayashi, H., Howard, J.B., and Sarofim, A.F., 1976, "Coal Devolatilization at High Temperatures," 16th Symp. (Int'l.) on Combustion, The Combustion Institute

Koryabkina, N.A., Phatak, A.A., Ruettinger, W.F., Farrauto, R.J., and Ribeiro, F.H., 2003, "Determination of Kinetic Parameters for the Water–Gas Shift Reaction on Copper Catalysts under Realistic Conditions for Fuel Cell Applications," Journal of Catalysis, Vol. 217, pp. 233-239

Kusar, H., Hocevar, S., and Levec, J., 2006, "Kinetics of the Water-Gas-Shift Reaction over Nanostructured Copper–Ceria Catalysts," Applied Catalysis B: Environmental, Vol. 63, pp. 194–200.

Ranz, W.E., and Marshall, W.R., 1952, "Evaporation from Drops Part 1 and Part 2," Chemical Engineering Progress, Vol. 48, pp. 173-180

Rase, H.F., *Chemical Reactor Design for Process Plants: Volume two – Case Studies and Design Data*, John Wiley and Sons, 1977.

Rhodes, C., Hutchings, G.J., and Ward, A.M., 1995, "WGSR: Finding the Mechanistic Boundary," Catalysis Today, Vol. 23, pp. 43-48.

Rhodes, C., and Hutchings, G.J., 2003, "Studies of the Role of the Copper Promoter in the Iron Oxide/ Chromia High Temperature Water Gas Shift Catalyst," Physical Chemistry Chemical Physics, Vol. 5, pp. 2719–2723

Salmi, T., and Hakkarainen, R., 1989, "Kinetic Study of the Low-Temperature Water-Gas-Shift Reaction over a Cu-ZnO Catalyst," Applied Catalysis, Vol. 49, pp. 285- 306

Sato, T., Kurosawa, S., Smith Jr., R.L., Adschiri, T., and Arai, K., 2004, "Water Gas Shift Reaction Kinetics under Noncatalytic Conditions in Supercritical Water," Journal of Supercritical Fluids, Vol. 29, pp. 113-119, 2004.

Silaen, A., and Wang, T., 2005, "Simulation of Coal Gasification Process Inside a Two-Stage Gasifier," Paper 20-1, Proceedings of the 22nd International Pittsburgh Coal Conference, Pittsburgh, Pennsylvania, September 19-22.

Silaen, A., and Wang, T., 2006, "Effect of Fuel Injection Angles on Performance of a Two-Stage Gasifier," Paper 20-4, presented at the 23rd International Pittsburgh Coal-Gen Conference, Pittsburgh, Pennsylvania, Sept. 25-28, 2006.

Silaen, A., and Wang, T., 2009, "Comparison of Instantaneous, Equilibrium and Finite Rate Gasification Models in an Entrained Flow Coal Gasifier," Paper 14-3, presented at the 26th International Pittsburgh Coal Conference, Pittsburgh, Pennsylvania, Sept. 21-24, 2009.

Silaen, A., and Wang, T., 2010, "Effect of Turbulence and Devolatilization Models on Gasification Simulation," International Journal of Heat and Mass Transfer, Vol. 53, pp. 2074-2091, 2010.

Silaen, A., and Wang, T., 2011, "Investigation of Coal Gasification Process under Various Operating Conditions Inside a Two-Stage Entrained Flow Gasifier", accepted for publication in ASME Journal of Thermal Science and Engineering Applications, 2011.

Smith, B., Loganathan, M., and Shanatha, M.S., 2010, "A Review of the Water Gas Shift Reaction Kinetics," International Journal of Chemical Reactor Engineering, Vol. 8.

Smoot, D.L., and Smith, P.J., 1985, "Coal Combustion and Gasification," Plenum Press

Sundararajan, A.T., and Shet, U.S.P., 2009, "Numerical Modeling of a Steam-Assisted Tubular Coal Gasifier," International Journal of Thermal Sciences, Vol. 48, pp. 308-321.

Tampa Electric Polk Power Station Integrated Gasification Combined Cycle Project, Final Technical Report, August 2002.

Twigg, M.V., 1989, *Catalyst Handbook*, second edition, Wolfe Publishing Ltd.

Wabash River Coal Gasification Repowering Project, Final Technical Report, August 2000.

Waind, T., and Whitty, K., 2010, "Characterization of a Small Scale Slurry-Fed, Oxygen-Blown Entrained Flow Gasifier: How Injector Geometry Affects Flame Stability and Performance," 2010 International Pittsburgh Coal Conference, Istanbul, Turkey October 11 – 14, 2010.

Wang, T., Silaen, A., Hsu, H.W., and Lo, M.C., 2006, "Partial Load Simulation and Experiments of a Small Coal Gasifier," Paper 20-3, presented at the 23rd International Pittsburgh Coal-Gen Conference, Pittsburgh, Pennsylvania, Sept. 25-28, 2006.

Wang, T., Silaen, A., Hsu, H.W., and Shen, C.H., 2007, "Effect of Slag Tap Size on Gasification Performance and Heat Losses in a Quench-type Coal," Paper 37-4, presented at the 24th International Pittsburgh Coal-Gen Conference, Johannesburg, South Africa, Sept. 10-14, 2007.

Wang, T., Silaen, A., Hsu, H.W., and Shen, C.H., 2010, "Investigation of Heat Transfer and Gasification of Two Different Fuel Injectors in an Entrained-Flow Gasifier," ASME Journal of Thermal Science and Engineering Applications, Vol.2, pp. 011001/1-10, March 2010.

Wang, T., Silaen, A., Hsu, H.W., and Shen, C.H., 2011, "Top Fuel Injection Design in an Entrained-Flow Coal Gasifier Guided by Numerical Simulations," ASME Journal of Thermal Science and Engineering Applications, Vol. 3, pp. 011009/1-8, March 2011.

Watanabe, H., and Otaka, M., 2006, "Numerical Simulation of Coal Gasification in Entrained Flow Coal Gasifier," Fuel, Vol. 85, pp. 1935-1943, 2006.

Watanabe, M., Mochiduki, M., Sawamoto, S., Adschiri, T., and Arai, K., 2001, "Partial Oxidation of N-Hexadecane and Polyethylene in Supercritical Water," J. Supercrit. Fluids, Vol. 20, pp. 257

Westbrook, C.K., and Dryer, F.L., 1981, "Simplified Reaction Mechanisms for the Oxidation of Hydrocarbon Fuels in Flames," Vol. 27, pp.31-43

Wheeler, C., Jhalani, A., Klein, E.J., Tummala, S., and Schmidt, L.D., 2004, "The Water-Gas-Shift Reaction at Short Contact Times," Journal of Catalysis, Vol. 223, pp. 191–199